Available online at www.sciencedirect.com
SCIENCE DIRECT®
Journal of Catalysis 225 (2004) 179–189
JOURNAL OF CATALYSIS
www.elsevier.com/locate/jcat

Mechanism and kinetics of the selective NO reduction over Co-ZSM-5 studied by the SSITKA technique
2. Reactivity of NO_x-adsorbed species with methane

E.M. Sadovskaya,[a] A.P. Suknev,[a] L.G. Pinaeva,[a] V.B. Goncharov,[a] B.S. Bal'zhinimaev,[a] C. Chupin,[b] J. Pérez-Ramírez,[b,1] and C. Mirodatos[b,*]

[a] *Boreskov Institute of Catalysis, pr. Lavrentieva, 5, 630090 Novosibirsk, Russia*
[b] *Institut de Recherches sur la Catalyse, 2 av. A. Einstein, F-69626 Villeurbanne cedex, France*

Received 3 January 2004; revised 17 March 2004; accepted 22 March 2004

Available online 12 May 2004

Abstract

Steady-state isotopic transient kinetic analysis (SSITKA) was applied to study the reactivity of adsorbed NO_x species with methane over Co-ZSM-5 during CH_4-SCR of NO at different partial oxygen concentrations. Numerical analysis of the isotope responses after switching from $^{14}N^{16}O$ to $^{15}N^{18}O$, from $^{16}O_2$ to $^{18}O_2$, from $^{12}CH_4$ to $^{13}CH_4$, and from $C^{16}O_2$ to $C^{18}O_2$ in the feed gas was performed. This enables determination of (i) the concentration of different forms of NO_x adspecies on Co sites, (ii) their reaction rates with methane, and (iii) the concentration of surface intermediates resulting from the interaction of NO_x species with methane. The NO reduction with CH_4 in the presence of oxygen was shown to proceed by two different pathways with participation of (1) $NO_2^{\delta+}$ species (formed on nanoclusters of cobalt oxide located inside the zeolite channels) and (2) NO_2^- nitrite complexes (formed on larger cobalt oxide particles located outside the zeolite channels), the reaction rate by the former being appreciably higher under the SCR reaction conditions studied. Mononitrosyl species appear not to be directly involved in the overall process. Modeling results indicate that the rate of the first route is limited by the interaction of $NO_2^{\delta+}$ species and adsorbed methane, while in the second route the formation of nitrite species is a rate-determining step. Based on the obtained results, an overall reaction mechanism of the CH_4-SCR of NO in the presence of oxygen is proposed.

Keywords: SSITKA; $deNO_x$; CH_4-SCR; Co-ZSM-5; Kinetics; Mechanism; Cobalt species; Active sites

1. Introduction

In the still widely open research area of NO selective catalytic reduction (SCR) by CH_4 instead of NH_3, Part I of our investigation elaborated on a mechanistic understanding of the transformations of NO with oxygen over an ion-exchanged Co-ZSM-5 catalyst [1]. From that study, the kinetics and mechanism of reactive $NO_2^{\delta+}$ species, active intermediates in the SCR of NO_x, as well as the number of active sites for NO adsorption and their possible location in the zeolite structure were elucidated. This information is essential to further investigate the elementary steps involved in the reaction of NO_x species with methane during $deNO_x$ CH_4-SCR in the presence of oxygen, which has been investigated in Part II.

From the mechanistic investigations reported in the literature, it is generally postulated that during SCR, surface NO_x species interact with methane to form surface intermediates, which are further converted and decomposed into the reaction products [2–14]. However, the detailed structure of these species is unclear. Many authors have speculated that nitrite–nitrate complexes are involved in the process [2–8]. However, Wang et al. [13,14] suggested that adsorbed NO species responsible for methane activation cannot be ascribed unambiguously to nitrite–nitrate complexes, and therefore denote these species as NO_y. In a previous in situ DRIFT (diffuse reflectance infrared Fourier trans-

* Corresponding author. Fax: +33 472 445399.
E-mail address: mirodatos@catalyse.univ-lyon1.fr (C. Mirodatos).
[1] On academic leave from Norsk Hydro, Agri Research Centre, Porsgrunn, Norway.

0021-9517/$ – see front matter
doi:10.1016/j.jcat.2004.03.032

form) spectroscopic investigation [15], we have observed that $NO_2^{\delta+}$ species were formed in addition to nitrite–nitrate complexes after NO adsorption in the presence of oxygen over Co-ZSM-5. The intensity of the band ascribed to $NO_2^{\delta+}$ species declined much more rapidly than the one of nitrite–nitrate and mononitrosyl species after methane addition to a $NO + O_2$ mixture at reaction temperature (400–500 °C). Multiple NO species on isolated Co ions like dinitrosyls were not identified under the conditions applied. Based on this key feature, another reaction route of NO reduction was proposed, involving these $NO_2^{\delta+}$ species as active intermediates able to react with activated forms of methane. A similar conclusion on the participation of $NO_2^{\delta+}$ species in the reaction with methane was proposed by Boix et al. [12].

In order to quantify the concentration and reactivity of the various NO_x adspecies potentially participating in the SCR with CH_4 under steady-state conditions, a SSITKA (steady state isotope transient kinetic analysis) technique has been applied. As a matter of fact, while DRIFT spectroscopy mostly detects "spectator" adspecies under steady-state conditions, SSITKA enables a quantitative determination of the concentration of adsorbed active intermediate species, as well as their rates of formation and consumption [16,17]. In Part I of this work [1], the dynamics of isotopic exchange between the $NO + O_2$ and the catalyst under adsorption/desorption equilibrium were investigated in the absence of reducing agent. Three types of adsorbed NO_x species were distinguished on Co sites, based on their rate of ^{15}N exchange with gaseous NO decreasing substantially among the following sequence: mononitrosyls $\gg$ $NO_2^{\delta+}$ species $>$ nitrite complexes. From the dynamics of this exchange, rate constants of their formation and decomposition were determined. In addition, by analyzing the dynamics of ^{18}O exchange between gaseous NO and the various pools of oxygen present in the catalyst, it was proposed that the high reactivity of $NO_2^{\delta+}$ species originates from its unique interaction with oligonuclear cobalt oxidic species and hydroxyl groups in the zeolite channels. On the contrary, either less reactive mononitrosyls on isolated cobalt ions or nitrite complexes on larger cobalt oxide particles located outside the zeolite framework or at defect interfaces would not play a major role in the SCR process. This indicates an essential participation of the zeolite matrix in the overall reaction.

In this paper, the dynamics of the above species have been investigated in the presence of methane using a SSITKA technique upon analysis of the isotopic responses $^{14}N^{16}O \rightarrow {}^{15}N^{18}O$, $^{16}O_2 \rightarrow {}^{18}O_2$, $^{12}CH_4 \rightarrow {}^{13}CH_4$, and $C^{16}O_2 \rightarrow C^{18}O_2$. The rate constants of NO_x reaction with methane were estimated from the differences between concentrations of NO_x adspecies determined under adsorption/desorption equilibria (i.e., in the absence of reducing agent) and under SCR conditions. The dynamics of ^{13}C-label transfer have been also investigated in order to determine the pathways of CO_2 formation as well as to estimate the concentrations of C,N-containing intermediate complexes. A detailed assessment of the different elementary steps involved enables identification of rate-determining steps in the overall SCR process and to evaluate the concentration of active cobalt species.

2. Experimental

2.1. Catalysts

The Co-ZSM-5 catalyst used in this study was prepared from Na-ZSM-5 (molar SiO_2/Al_2O_3 ratio = 37) by an ionic exchange technique with a $Co(NO_3)_2$ solution followed by drying and calcination at 500 °C [1,8]. The cobalt content in Co-ZSM-5 was 1.8 wt% that corresponds to 1.9×10^{20} at.Co/g_{cat}, i.e., to a degree of exchange (DE) of 292%, by considering the total number of exchange sites per ZSM-5 unit cell being equal to half the number of Al atoms per unit cell (one Co^{2+} for two H^+, i.e., $Co_{x/2}Al_xSi_{96-x}O_{192}$,16$H_2O$) [18]. Though no crystalline cobalt oxide phases (CoO or Co_3O_4) were detected by X-ray diffraction spectroscopy, indicating that the size of cobalt oxide particles did not exceed 30–40 Å, it was shown from XPS and TEM studies [18] that different cobalt forms coexist in the catalyst, including: (i) Co oxides particles (Co_xO_y) at the external surface of the zeolite crystals, (ii) oligonuclear or nanoclusters of cobalt oxide inside the zeolite pores, formed of tetrahedral Co^{2+} ions agglomerated with O^{2-} ions, most likely located at the intersection of straight and zig-zag channels, and (iii) isolated tetrahedral and octahedral cobalt ions Co^{2+} located at ion-exchange sites. Sieved 0.3- to 0.5-mm particles were used in the present study, after checking that no external mass transfer (or extraparticle) limitation occurred (no change in conversion as a function of particle size). Occurrence of internal mass transfer limitation (intracrystalline diffusion) will also be discarded, as discussed later (see Discussion).

2.2. SSITKA experiments

SSITKA experiments were carried out as follows: when the steady state was achieved under $NO + CH_4 + O_2 + He$ flow, the gas mixture was replaced stepwise by the same one containing isotopically labeled molecules: (i) doubly labeled nitric oxide $^{15}N^{18}O$ containing 94.6% of ^{15}N and 92.9% of ^{18}O, (ii) labeled oxygen $^{18}O_2$ containing 99% of ^{18}O, and (iii) labeled methane $^{13}CH_4$ containing 98% of ^{13}C. The catalyst was loaded in a packed-bed reactor, consisting of a high thermo-conductive tube with internal diameter of 3 mm and length of 120 mm. In order to determine whether the reactor behavior can be described as a plug flow, 1 vol% of argon was added into the feed gas containing the isotope molecules. Table 1 shows the experimental conditions in the various isotopic switches carried out: $^{14}N^{16}O \rightarrow {}^{15}N^{18}O$, $^{16}O_2 \rightarrow {}^{18}O_2$, $^{12}CH_4 \rightarrow {}^{13}CH_4$, and $C^{16}O_2 \rightarrow C^{18}O_2$. The last isotopic switch was performed to analyze a possible isotope

Table 1
Experimental conditions during the transient isotopic switches in SSITKA at 450 °C and 1 bar

	$^{14}N^{16}O \rightarrow {}^{15}N^{18}O$	$^{16}O_2 \rightarrow {}^{18}O_2$	$^{12}CH_4 \rightarrow {}^{13}CH_4$	$C^{16}O_2 \rightarrow C^{18}O_2$
W, g	0.23	0.1	0.1	0.1
F, ml/min	120	100	120	60
GHSV, 1/h	15,000	30,000	36,000	18,000
Feed,[a] vol%	NO: 0.6	NO: 0.95	NO: 0.3	CO_2: 2
	CH_4: 0.75	CH_4: 1.1	CH_4: 0.3–0.6	
	O_2: 0.15–3	O_2: 5	O_2: 3	

[a] He was used as the balance gas.

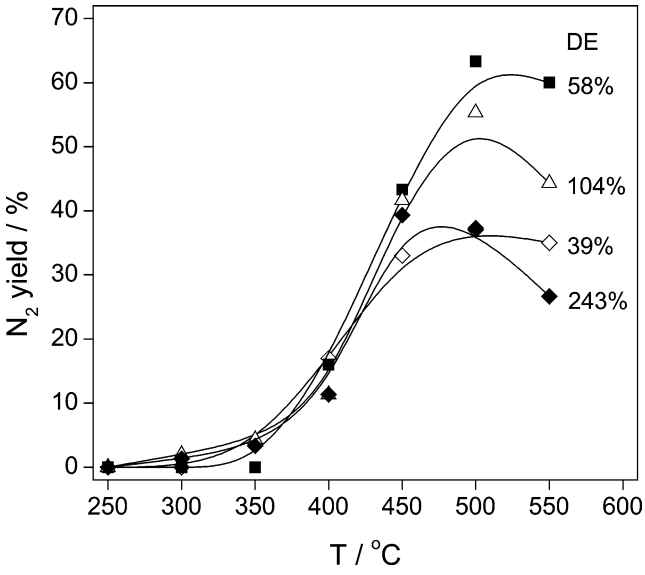

Fig. 1. N_2 yield vs temperature during deNO_x HC-SCR over Co-ZSM-5 at different ion-exchange degrees (DE) of cobalt. Conditions: 0.1 vol% NO + 0.25 vol% CH_4 + 5 vol% O_2 in He; GHSV = 8000 h^{-1}; $P = 1$ bar [18].

exchange of reaction products in the catalyst. The temperature in these experiments was 450 °C, which was shown previously [15] to correspond for overexchanged zeolites to the optimized concentration of reactive $NO_2^{\delta+}$ species before methane admission, therefore, to the maximum N_2 yield obtained under CH_4-SCR of NO conditions. As a matter of fact, a typical N_2 yield was about 45%, as shown in Fig. 1 from [18], with 50% NO conversion and 90% N_2 selectivity and a marginal selectivity to NO_2 of 10%, since N_2O was never detected under our reaction conditions. Depending on the inlet methane and oxygen concentration, the conversion of CH_4 conversion into CO_2 and H_2O ranges from 30 to 60%.

The gas composition at the reactor outlet was continuously analyzed with a quadrupole mass spectrometer VG Sensorlab 200D, which can monitor 16 masses simultaneously. The mass spectrometric data were quantified using fragmentation patterns determined experimentally from calibration gases. The concentrations of $H_2{}^{18}O$, $^{14}N^{15}N$, $^{15}N^{16}O$, $^{15}N^{18}O$, $^{16}O^{18}O$, $^{18}O_2$, $C^{16}O_2$, $C^{16}O^{18}O$, and $C^{18}O_2$ were determined from the intensities of parent peaks at m/e 20, 29, 31, 33, 34, 36, 44, 46, and 48, respectively, and the concentrations of CH_4 and $H_2{}^{16}O$ from the intensities of peaks at m/e 15 and 17, respectively. Mass m/e 46 corresponds to labeled $C^{16}O^{18}O$, after correction from the side NO_2 formation. The concentration of $^{14}N_2$ was calculated by subtraction of the known contribution of $C^{16}O_2$ and $C^{16}O^{18}O$ from the intensity at m/e 28 (under excess oxygen, CO formation is negligible [18]). The respective contributions from $^{14}N^{16}O$ and $^{15}N_2$ ($m/e = 30$) as well as from $^{16}O_2$ and $^{14}N^{18}O$ (m/e = 32) were determined taking into account that the total (chemical) concentration of each compound does not change in the course of SSITKA experiments. Since NO_2 concentration was very low during the experiments (less than 0.5% from that of NO), its contribution into m/e 30 was neglected. In the experiments with labeled $^{13}CH_4$, the concentrations of H_2O, NO, O_2, $^{12}CO_2$, and $^{13}CO_2$ were determined from intensities of parent peaks at m/e 18, 30, 32, 44, and 45, respectively. The concentrations of N_2 and $^{13}CH_4$ were calculated by subtracting the contributions of CO_2 and H_2O from intensities at m/e 28 and 17, respectively, and the concentration of $^{12}CH_4$ was determined by subtracting the contribution of $^{13}CH_4$ from the intensity at m/e 15.

2.3. Numerical analysis of SSITKA responses

The model of isotope transfer carried out under steady-state reaction proceeding in a plug-flow reactor can be written by the system of hyperbolic differential equations,

$$\frac{\partial C_i\alpha_i}{\partial t} + \frac{U}{V}\frac{\partial C_i\alpha_i}{\partial \xi} = -\frac{G}{VN}\left(\alpha_i \sum_{k=1}^{N_{i_1}} \vec{w}_{ik} - \sum_{l=1}^{N_{i_2}} \overleftarrow{w}_{il}\alpha_l\right),$$

$$\theta_j \frac{\partial \alpha_j}{\partial t} = \alpha_j \sum_{k=1}^{N_{j_1}} \vec{w}_{jk} - \sum_{l=1}^{N_{j_2}} \overleftarrow{w}_{jl}\alpha_l,$$

with initial conditions,

$$t = 0: \quad \alpha_i = \alpha_i^0,\ \alpha_j = \alpha_j^0$$

$$\xi = 0: \quad \alpha_i = \alpha_i^{\text{input}}.$$

The significance of the various parameters is listed in under Notation. The model takes into account the change in isotope-label concentration in the reactants and products and surface intermediate both in time and axial coordinate along the catalytic bed.

The various parameters were determined by the minimization of root-mean-square deviation of experimental data

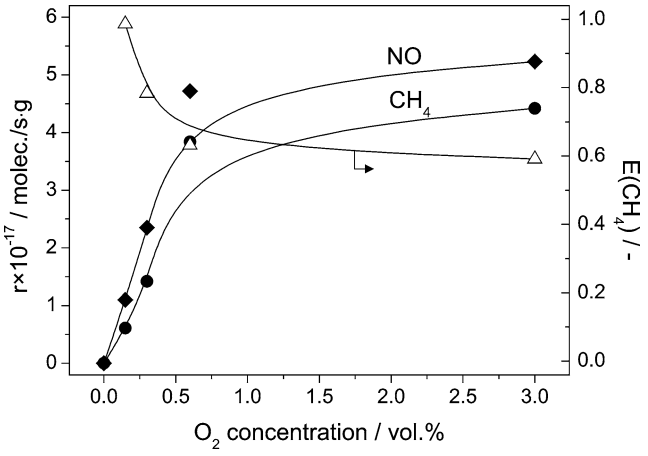

Fig. 2. Reaction rates of (◆) NO and (●) CH_4 and (△) hydrocarbon efficiency during deNO_x HC-SCR over Co-ZSM-5 at different O_2 concentrations. Conditions: 0.6 vol% NO + 0.75 vol% CH_4 + 0–3 vol% O_2 in He; $T = 450\,^{\circ}C$; GHSV = 15,000 h^{-1}; $P = 1$ bar.

from calculated ones,

$$F(\bar{\vartheta}) = \sum_{l=1}^{n} \int_0^T \left(\alpha_l(t,\bar{\vartheta}) - \alpha_l^{\exp}(t)\right)^2 \mathrm{d}t \to \min,$$

where $\alpha_l^{\exp}(t)$ and $\alpha_l(t,\bar{\vartheta})$ are the experimental and calculated dependencies of isotope fractions in the reactants and products, respectively. The Newton algorithm of functional minimization was used, and the differential equations were solved by the difference method, as described in [19].

3. Results

3.1. Steady-state reaction rate and hydrocarbon efficiency

The overall reactions of SCR of NO with methane in the presence of oxygen and of direct methane oxidation can be written as follows:

$$2NO + CH_4 + O_2 \to N_2 + CO_2 + 2H_2O, \quad (1)$$

$$CH_4 + 2O_2 \to CO_2 + 2H_2O. \quad (2)$$

From the above equations, the efficiency of methane in the SCR process can be expressed as the ratio of N_2 and CO_2 outlet concentrations, $E(CH_4) = [N_2]_{out}/[CO_2]_{out}$. $E(CH_4)$ varies between 1, which corresponds to a pure SCR process without methane oxidation with O_2 [Eq. (1)] and 0, which corresponds to a pure methane oxidation process [Eq. (2)] without NO reduction.

Fig. 2 shows the steady-state reaction rates of NO reduction and CH_4 oxidation as a function of the oxygen content in the reaction mixture.

The rates of NO and CH_4 conversion dramatically increase in the O_2 concentration range between 0–0.6 vol%. At higher oxygen concentrations the reaction rates experience slight changes. The hydrocarbon efficiency was close to 1 at low oxygen concentration and strongly declined as the O_2 content increased, reaching the value of 0.6 for 3 vol% of O_2. The side concentration of NO_2, probably associated with the decomposition of nitrite species on cobalt oxide particles (mostly located outside the zeolite matrix [18]), will not be considered further in this paper.

3.2. Switch from $^{14}N^{16}O$ to $^{15}N^{18}O$ in $NO + CH_4 + {}^{16}O_2 + He$

Fig. 3a shows the changes in ^{15}N isotope fraction in NO at the reactor outlet at different O_2 concentrations in comparison with the response curve of argon, added to the mixture containing the $^{15}N^{18}O$ isotope.

A delay of 2 s is observed for Ar appearance in the gas phase after the isotopic switch, which corresponds to the residence time of inert gas in the system composed between

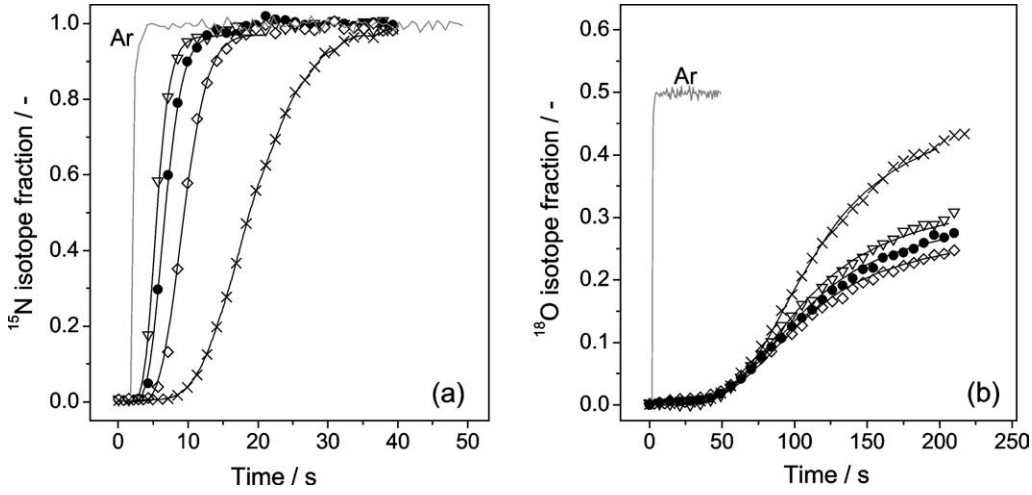

Fig. 3. Experimental (symbols) and simulated (lines) isotopic fractions of (a) ^{15}N and (b) ^{18}O in NO compared to the Ar response vs time upon switching from $^{14}N^{16}O$ to $^{15}N^{18}O$ in 0.6 vol% NO + 0.75 vol% CH_4 + O_2 + He flow (solid lines) at (▽) 0.15 vol%, (●) 0.6 vol%, (◇) 3 vol% O_2, and (×) 0.6 vol% NO + 3 vol% O_2 in He. Conditions in Table 1.

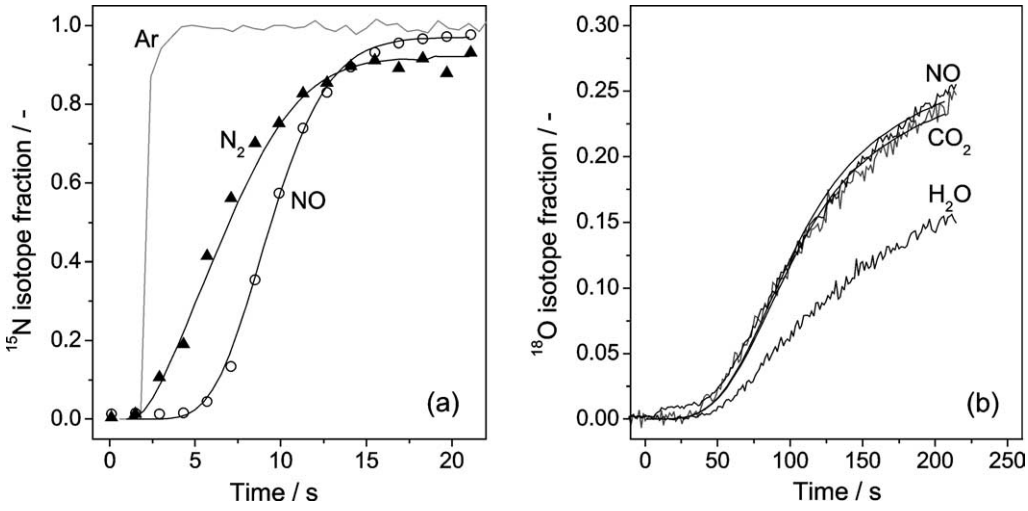

Fig. 4. Isotopic fractions of (a) ^{15}N in NO and N_2 compared to the Ar response and (b) ^{18}O in NO, CO_2, and H_2O vs time upon switching from $^{14}N^{16}O$ to $^{15}N^{18}O$ in 0.6 vol% NO + 0.75 vol% CH_4 + 3 vol% O_2 in He. Conditions in Table 1.

the switching valve and the mass spectrometer, therefore including reactor and tubing. The stepwise shape of the Ar response curve indicates in addition that this reactor can be well described with a plug-flow model. The ^{15}N concentration within the nonreacted NO at the reactor outlet is shifted by several seconds from the Ar signal, suggesting that there is a pool of reversibly adsorbed NO species onto the catalyst, in fast exchange with the gas phase. The observed delay corresponds to the mean residence time of the reactant in this reversible pool. Similar delayed response curves ($\times$ in Fig. 3a) were obtained in the SSITKA experiments in the absence of methane, i.e., under adsorption/desorption equilibrium [1]. It was shown for this case that a first pool of nitrogen atoms in fast exchange with the gas phase was formed of cobalt mononitrosyls, as being the most rapidly formed and weakly bound NO_x species. Then the nitrogen label was also exchanging in the pool of $NO_2^{\delta+}$ species and then of nitrite complexes. The rates of isotope replacement in mononitrosyls and $NO_2^{\delta+}$ species were found to be similar, whereas the replacement rate in nitrite complexes was one order of magnitude lower. This results in a very slow return of the ^{15}N concentration in outlet NO to a steady state corresponding to ^{15}N-label content in inlet NO.

In the presence of methane (SCR), one can see that the ^{15}N label appears much earlier in the unconverted NO gas phase and its concentration increases more rapidly in comparison with what is observed in the absence of methane, under adsorption/desorption equilibrium (compare $\diamond$ and $\times$ in Fig. 3a). This means that the amount of weakly bounded NO_x species participating in the fast isotope exchange with NO (i.e., mononitrosyls and $NO_2^{\delta+}$ species) strongly decreases under reaction conditions. In addition, the very slow relaxation at the end of the transient curves in the absence of methane, which was attributed to nitrite complexes [1], is not observed under SCR conditions, indicating that the concentration of the latter species is very low in the presence of methane. As expected, the labeled atoms from $^{15}N^{18}O$ were also transferred to the reaction products after the SSITKA switch.

In Fig. 4a the ^{15}N label appears in N_2 at the reactor outlet earlier than in the unconverted NO, the isotopic fraction of ^{15}N in N_2 remaining higher than the one in NO for at least 10 s ($\alpha^{15}_{N_2} > \alpha^{15}_{NO}$). Such an effect may be easily explained taking into account the plug–flow behavior in our reactor. As seen below, the unconverted NO reactant is in fast and reversible adsorption equilibrium with the catalyst forming a large pool of reversible adspecies, as cobalt mononitrosyls and $NO_2^{\delta+}$ species, delaying the label appearance at the reactor outlet. If in the mean time, part of adsorbed NO is transformed into a product, N_2, which immediately desorbs into the gas phase, the labeled molecules of the product (^{15}N in N_2) will appear almost from the beginning of the transient switch, i.e., as soon as the isotopic label of the reactant penetrates the reversible pool of adsorbed reactant in the inlet part of the catalytic bed (^{15}N in NO_{ads}).

Comparison of the dynamics of labeled nitrogen and oxygen transfer in Figs. 4a and b, respectively, indicates that the ^{18}O label appears in the unconverted NO significantly later than ^{15}N (approximately 5 vs 50 s, respectively) and at a very low rate, even more slowly than in the absence of methane (by comparing $\diamond$ and $\times$ in Fig. 3). This slow transfer of ^{18}O from NO reactant is also observed in CO_2 at a rate close to that observed for NO but at a still lower rate for H_2O (Fig. 4b). This can be ascribed to the secondary oxygen exchange between the relatively small pool of NO_x species and the large pool of exchangeable oxygen atoms belonging to the zeolite lattice [1]. The instantaneous rate of labeled oxygen transfer into the zeolite lattice can be calculated by subtracting the amount of ^{18}O atoms at the reactor outlet (summing label concentrations in NO, CO_2, and H_2O) from that at the reactor inlet. This rate was slightly higher under the reaction conditions than under adsorption/desorption equilibrium at the same NO and O_2 concentrations (8.4×10^{17} and 7.7×10^{17} molec/(g s), respectively, at 200 s). Despite the

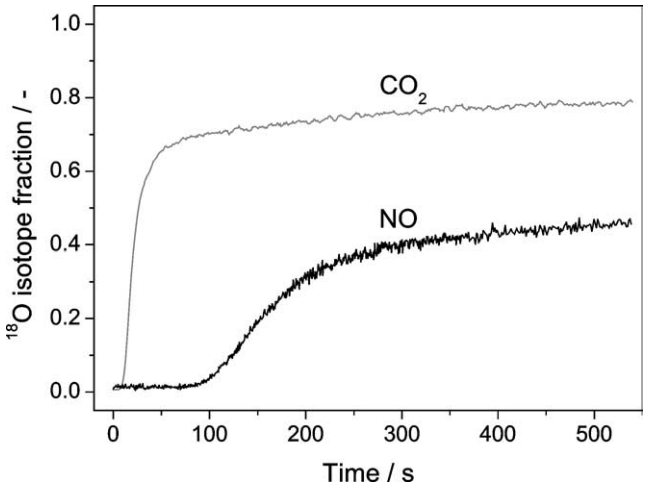

Fig. 5. Isotopic fraction of ^{18}O in NO and CO_2 vs time upon switching from $^{14}N^{16}O$ to $^{15}N^{18}O$ in 1.2 vol% NO in He and from $C^{16}O_2$ to $C^{18}O_2$ in 2 vol% CO_2 in He, respectively. Conditions in Table 1.

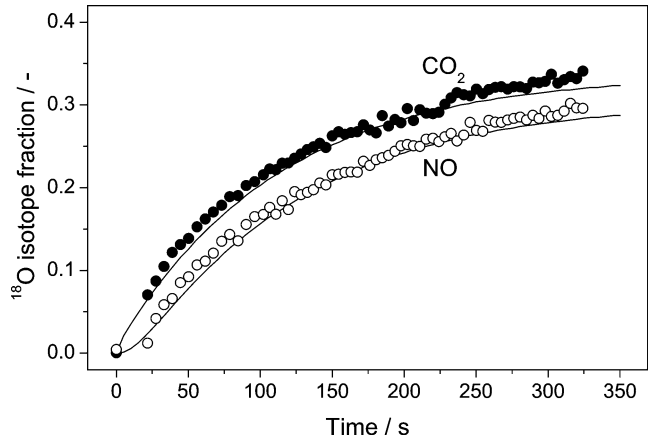

Fig. 6. Experimental (points) and simulated (lines) isotopic fractions of ^{18}O in (○) NO and (●) CO_2 vs time upon switching from $^{16}O_2$ to $^{18}O_2$ in 0.95 vol% NO + 1.1 vol% CH_4 + 5 vol% O_2 in He. Conditions in Table 1.

large amount of labeled oxygen transferred into the catalyst, no ^{18}O is transferred into gas-phase oxygen (either as $^{18}O_2$ or $^{16}O^{18}O$), which means that all the steps involving activation and interaction of O_2 with NO_x proceed irreversibly.

The slow transfer of labeled oxygen within the oxygen-containing products CO_2 and H_2O as noted above obviously reflects the reversible interaction between these polar molecules and the zeolite pool of oxygen (Fig. 4b). As a result of this oxygen exchange the label concentration in the reaction products declines along the catalyst bed, but not so sharply as that in NO.

3.3. Switch from $C^{16}O_2$ to $C^{18}O_2$ in CO_2 + He

In order to gain more insight into the interaction between the reaction products and the catalyst surface, a SSITKA switch from $C^{16}O_2$ to $C^{18}O_2$ was carried out in a 2 vol% CO_2 + He flow (see Table 1), and compared to the already described NO switch response, as depicted in Fig. 5.

The ^{18}O label in the CO_2 gas phase appears and stabilizes much faster than in the case of NO (Fig. 5). This means that the rate of ^{18}O exchange between the CO_2 and the catalyst is not negligible, though considerably lower than that for NO. As a consequence, the oxygen exchange which occurs between the reaction products and the catalyst superimposes with the initial (as formed) content of oxygen label in the products. Therefore no straightforward conclusion on the mechanism of ^{18}O label transfer into the reaction products can be derived from the shape of isotope responses. To this end, the rate of isotope exchange between the reaction products and the catalyst should be computed, and then the mechanism of oxygen transfer could be assessed using numerical analysis of the isotope responses.

3.4. Switch from $^{16}O_2$ to $^{18}O_2$ in $^{14}N^{16}O + CH_4 + O_2$ + He mixture

When $^{16}O_2$ is switched to $^{18}O_2$ in the overall steady-state NO + CH_4 + O_2 + He mixture, the transient concentration of ^{18}O label within the unconverted oxygen follows strictly the inert Ar response (as shown in Fig. 3), confirming that no reversible oxygen dissociates on the catalyst. Fig. 6 shows the ^{18}O transfer from gaseous oxygen to CO_2 together with the transfer to unconverted NO. In this experiment, the ^{18}O transfer from gaseous oxygen to H_2O was not recorded.

It can be seen that ^{18}O label appears in NO with a delay of about 15 s after CO_2 (Fig. 6), which can result only from isotope exchange of NO with the large pool of catalyst oxygen atoms. In fact, a substantial part of labeled oxygen is transferred into the catalyst as concluded from the comparison between the amount of $^{18}O_2$ consumed with that of ^{18}O atoms at the reactor outlet. Since participation of molecular oxygen in isotopic exchange with the catalyst oxygen is negligible (as shown above and in [1]), it is unclear at this stage how ^{18}O-label transfer into the catalyst proceeds during the catalytic reaction or as a result of CO_2 and H_2O re-adsorption and why ^{18}O label does not appear into NO immediately, but with a substantial delay. Numerical analysis of ^{18}O isotope responses was carried out to further elucidate these aspects (Section 3.6).

3.5. Switch from $^{12}CH_4$ to $^{13}CH_4$ in NO + CH_4 + O_2 + He mixture

Fig. 7 shows the dynamics of ^{13}C label transfer into CH_4 and CO_2 as compared with the response curve of argon.

A delay of ca. 1 s of isotope response in methane relative to that of argon was observed. Labeled ^{13}C appeared in CO_2 simultaneously with that in CH_4, but its concentration increased considerably slower. The slight shift of methane response relative to argon indicates a minor accumulation of reversible methane, most likely loosely bounded within the

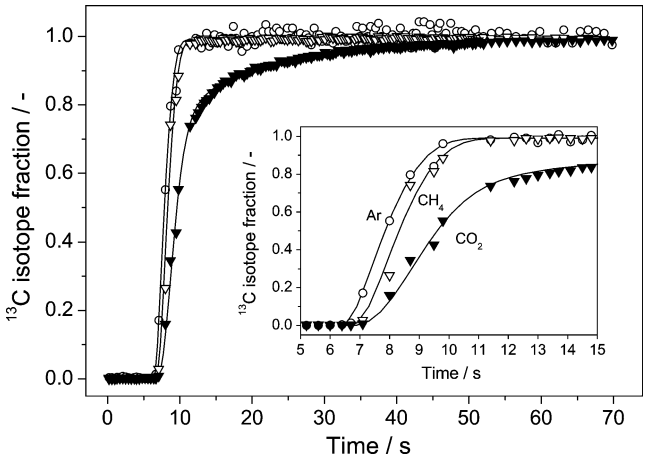

Fig. 7. Experimental (points) and simulated (lines) isotopic fractions of ^{13}C in CH_4 (▽) and CO_2 (▼) compared to the Ar response (○) vs time after switching from $^{12}CH_4$ to $^{13}CH_4$ in 0.3 vol% NO + 0.4 vol% CH_4 + 3 vol% O_2 in He. Conditions in Table 1.

zeolite matrix. In turn, the chemical interaction of methane with the catalyst to form reacting intermediates seems to be irreversible. The concentration of these carbon-containing intermediates will be determined from numerical simulation. Another important observation can be made from the dynamics of CO_2 isotope response. In Fig. 7, it can be seen that relatively fast increase of CO_2 isotope fraction proceeds for the initial period of time followed by pronounced deceleration relative to exponential dependence. This result strongly suggests that CO_2 does not originate from a single pathway but several routes leading to CO_2 proceed with different reaction rates.

3.6. Simulation results

3.6.1. Nitrogen labeling

According to our previous results [1], ^{15}N label can transfer from NO into three types of adsorbed NO_x species: mononitrosyls adsorbed on cobalt ions, $NO_2^{\delta+}$ species adsorbed on oligonuclear oxide cobalt species in the channels, with participation of hydroxyl groups in the zeolite, and nitrite complexes adsorbed on larger cobalt oxide particles. Taking into account possible participation of all these complexes in N_2 formation, a general scheme of ^{15}N-label transfer under reaction conditions can be considered (Scheme 1), where $[z\text{-}^*N]_1$, $[z\text{-}^*N]_2$ and $[z\text{-}^*N]_3$ are the concentrations of all intermediate complexes resulting from the conversion of mononitrosyls NO, adsorbed $NO_2^{\delta+}$ species, and nitrite complexes (NO_2^-), respectively, into N_2.

This scheme accounts for an eventual isotope exchange between mononitrosyl and nitrite complexes but excludes the exchange of both complexes with $NO_2^{\delta+}$ species, because they are located on different active sites. As a matter of fact, mononitrosyls and nitrites can be formed on isolated ions and/or cobalt oxide particles, respectively, while formation of adsorbed $NO_2^{\delta+}$ requires the interface between the nanoclusters and zeolite lattice [1,18]. The rates of ad-

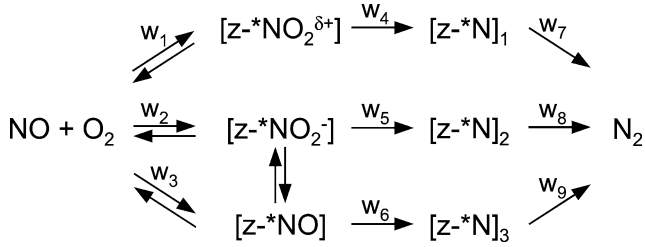

Scheme 1. Pathways for ^{15}N-label transfer under SCR reaction conditions where $[z\text{-}^*N]_1$, $[z\text{-}^*N]_2$ and $[z\text{-}^*N]_3$ are the concentrations of all intermediate complexes allowing the conversion of *NO, $^*NO_2^{\delta+}$, and $^*NO_2^-$ adspecies into N_2.

sorption/desorption steps in the absence of reducing agent can be expressed by means of the corresponding rate constants determined in [1] ($w_i = k_i C_{NO}$, $w_{-i} = k_{-i}\theta_i$). Since the dynamics of ^{15}N label switch in NO is determined by the formation and desorption rates of NO_x species (steps 1–3 in Scheme 1), this process can be described with the concentrations of NO_x species (θ_i) as the only unknown parameters. These parameters were fitted to the experimental data according to the procedure described elsewhere [19]. The calculated concentrations of the various adsorbed NO_x species obtained both under adsorption/desorption equilibrium in the absence of methane (from [1]) and under SCR reaction conditions (at the same NO and O_2 inlet concentrations) are reported in Table 2.

As can be seen, the concentration of cobalt mononitrosyls was ca. 15% lower under the reaction conditions than under adsorption/desorption equilibrium. This corresponds to the decrease of NO concentration in the gas phase during SCR (length-averaged drop of this value is also close to 15%). Therefore, adsorption–desorption equilibrium between NO in the gas phase and mononitrosyl adspecies is kept established under SCR conditions, and the rate of mononitrosyl conversion due to the SCR reaction is negligible compared to the rates of their formation and desorption. For this reason, the mononitrosyl contribution to the total NO conversion into N_2 remains marginal and its accurate estimation is not possible.

In contrast to mononitrosyls, the sharp decrease of $NO_2^{\delta+}$ and nitrite concentrations in the presence of methane (SCR conditions) as compared to adsorption/desorption equilibrium conditions exceeds considerably what could be assigned to the ∼ 15% decrease in NO concentration in the gas phase (Table 2). This clearly indicates the participation of these adspecies in the reaction. Since $NO_2^{\delta+}$ species and nitrite complexes are located on different active sites, the SCR reaction with a participation of $NO_2^{\delta+}$ and nitrites adspecies is most likely to proceed via parallel routes, both including a reaction step with methane.

Quite reliable estimations of the rates of $NO_2^{\delta+}$ and nitrite conversion were obtained from the differences between their adsorption and desorption rates (Table 2). The sum of these rates was found to be close to the total rate of N_2 formation. Then, one can conclude based on the balance ratio

Table 2
Estimated values of NO_x adsorbed species concentrations and the rates of their conversion in the SCR reaction

Oxygen inlet concentration, vol%	Concentration of adsorbed NO_x species, [molec/g] $\times 10^{-19}$						SCR reaction rate, [molec/(g s)]$\times 10^{-19}$		
	Adsorption–desorption (in the absence of CH_4)			SCR reaction (in the presence of CH_4)					
	[z-*NO]	[z-*$NO_2^{\delta+}$]	[z-*NO_2^-]	[z-*NO]	[z-*$NO_2^{\delta+}$]	[z-*NO_2^-]	[z-*NO]	[z-*$NO_2^{\delta+}$]	[z-*NO_2^-]
0.3	0.64	0.85	0.11	0.61	0.3	$\leqslant 0.1$	0	0.006	0.002
0.6	0.64	1.05	0.15	0.56	0.8	$\leqslant 0.1$	0	0.016	0.006
3	0.64	1.90	0.53	0.55	1.2	$\leqslant 0.1$	0	0.020	0.008

that the rate of N_2 formation via direct interaction of cobalt mononitrosyls with methane is negligible with respect to the other two pathways.

Numerical analysis of the dynamics of N_2 isotope replacement also enables the estimation of the total concentration of surface CNO_xH_y complexes, formed after $NO_2^{\delta+}$ and nitrites adspecies interaction with activated methane adspecies (noted $[z\text{-}^*N]_1$ and $[z\text{-}^*N]_2$ in Scheme 1). This concentration is about 20% of that of $NO_2^{\delta+}$ species in all the experiments (not reported in Table 2 for sake of clarity). As shown in Fig. 4a, a good agreement was found between the experimental and the calculated dynamic responses.

3.6.2. Carbon labeling

Numerical analysis of ^{13}C-label transfer confirms the involvement of two pathways involving activated CH_4 species during the SCR of NO_x. As a matter of fact, the calculated isotope responses were found not fitting with the experimental ones in the case of one-step or consecutive scheme of label transfer. The only satisfying agreement between the experimental and the calculated responses was obtained in the case of a parallel scheme of ^{13}C-label transfer with two pathways (Scheme 2), where $[z\text{-}^*C]_1$ and $[z\text{-}^*C]_2$ are the concentrations of all intermediate complexes resulted from CH_4 conversion into CO_2, with reaction rates r_1 and r_2, respectively.

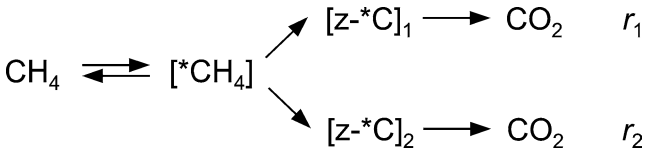

Scheme 2. Parallel pathways for ^{13}C-label transfer under SCR reaction conditions, where [*CH_4] is reversibly adsorbed methane, $[z\text{-}^*C]_1$ and $[z\text{-}^*C]_2$ are the concentrations of all intermediate complexes resulted from CH_4 irreversible conversion into CO_2, with reaction rates r_1 and r_2, respectively (most likely involving methoxy species OCH_3).

Table 3 shows the rates of CO_2 formation by the both routes. One can see that the reaction rates increase as the CH_4 concentration in the feed gas increases, but the ratio $r_1/r_2 = 2.3$ does not change. This ratio is close to that between the reaction rates for $NO_2^{\delta+}$ species and nitrite complexes ($0.020/0.008 = 2.5$). The concentrations of adsorbed species formed during methane conversion to CO_2 ($[z\text{-}^*C]_1$ and $[z\text{-}^*C]_2$) were also determined (Table 3). The proper nature of these adsorbed species or reacting intermediates will be discussed later on.

3.6.3. Oxygen labeling

From the simulation of the experiments with labeled oxygen ($N^{18}O$ and $^{18}O_2$), it was concluded that the observed rate of ^{18}O isotope replacement in CO_2 can be described with a two-step scheme of isotope exchange $CO_2 \leftrightarrow [O_{sur}] \leftrightarrow [O_{bulk}]$, $[O_{sur}]$ being the oxygen pool formed by the adsorption/desorption active sites (cobalt oxide particles and nanoclusters) and $[O_{bulk}]$ being the oxygen pool formed by the zeolite oxygen framework. This isotope exchange is limited by the rate of label transfer from the adsorption sites (O_{sur}) into the zeolite bulk (O_{bulk}). Taking into account that ^{18}O distribution in CO_2 and H_2O is close to equilibrium, it can be proposed that isotope exchange between the catalyst oxygen and the H_2O proceeds on the same sites as the exchange with CO_2 (most probably on hydroxyl groups of the zeolite), and is also limited by the label transfer from OH groups into the oxygen pool of the zeolite framework. Then, one can roughly estimate highest possible total rate of ^{18}O label transfer from CO_2 and H_2O into the catalyst under the reaction conditions. Numerical analysis of ^{18}O label transfer under the reaction conditions was performed for the experiments with both labeled $^{15}N^{18}O$ and labeled $^{18}O_2$. Numerical analysis of the experiments with labeled oxygen showed that isotope exchange with the reaction products cannot account for the observed acceleration of the label transfer; i.e., there are other pathways of ^{18}O-label trans-

Table 3
Estimated concentrations of carbon containing reacting intermediates $[z\text{-}^*C]_1$ and $[z\text{-}^*C]_2$ and rates of reaction into CO_2

Expt.	Feed composition, vol%			Surface concentration, [molec/g]$\times 10^{-19}$		Reaction rate, [molec/(g s)]$\times 10^{-19}$		r_1/r_2
	NO	O_2	CH_4	$[z\text{-}^*C]_1$	$[z\text{-}^*C]_2$	r_1	r_2	
1	0.3	3.0	0.3	0.016	0.084	0.019	0.008	2.4
2	0.3	3.0	0.4	0.022	0.010	0.025	0.011	2.3
3	0.3	3.0	0.6	0.026	0.015	0.031	0.014	2.2

port from gas-phase O_2 into the catalyst surface. The same conclusion can be drawn from the simulation results of the experiments with labeled NO: a new pathway of the label transfer from NO into the catalyst appeared in addition to the exchange with the reaction products and with adsorbed NO_x complexes. Considering different schemes of ^{18}O-label transfer, we had in mind two facts: the absence of reverse label transfer from the catalyst into O_2 as well as the absence of isotope exchange between O_2 and the catalyst under adsorption-desorption equilibrium (i.e., in NO + O_2 + He mixture in the absence of methane). The most probable way to explain these facts is to permit the label transfer on the step of active sites reoxidation. As concluded in [1], the pathway leading to $NO_2^{\delta+}$ formation is preceded by the oxidation of the active sites. Then, supposing that both oxygen atoms from these complexes participate in the reaction products formation and that the active sites can be reoxidized by both O_2 and NO (with the reoxidation rate being equal to the rate of these complexes conversion) we described well the dynamics of ^{18}O transfer in the experiments with both labeled NO and labeled oxygen (see Figs. 3b and 6).

4. Discussion

4.1. Internal diffusion limitation analysis

Before discussing the possible mechanistic pathways from the SSITKA results and modeling, the possibility of intracrystalline mass-transfer effects has to be considered since it might alter the ratio between the reaction rates via different pathways (with participation of $NO_2^{\delta+}$ and NO_2^- species). From the kinetics of NO_x adspecies formation previously reported in [1], the measured rate constant of NO adsorption allows us to estimate (by smallest extreme) the values of NO diffusion coefficient for the studied catalyst: $D_{NO}/L^2 \gg 50\ s^{-1}$ (where L is molecule radius). Since kinetic radiuses of NO and CH_4 molecules are close, their diffusion coefficients are also comparable. From the measured rate of methane consumption and concentration of NO_x complexes, the effective rate constant of CH_4 interaction with NO_x can be estimated. These values are about $10\ s^{-1}$, which is considerably lower than D_{CH_4}/L^2. Hence, any internal mass-transfer effects can be considered as negligible in the present study.

4.2. Main mechanistic pathways

Two types of SSITKA experiments, investigating the transfer of ^{15}N from NO to N_2 and the transfer of ^{13}C from CH_4 to CO_2, have independently shown that the formation of N_2 and CO_2 during CH_4-SCR of NO over Co-ZSM-5 proceeds via by two parallel routes. The rates of these routes are similar, as estimated from the ^{15}N and ^{13}C data. N_2 formation proceeds essentially via adsorbed $NO_2^{\delta+}$ species and nitrite complexes (NO_2^-). These adspecies are located on different active sites [1]: $NO_2^{\delta+}$ species are specifically

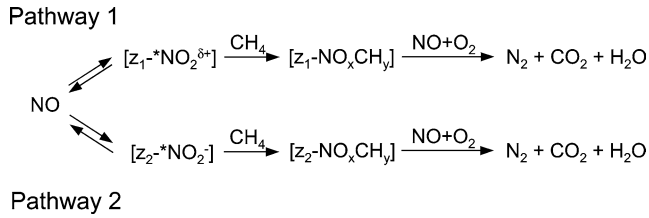

Scheme 3. Two main parallel pathways allowing the CH_4-SCR of NO into N_2 over Co-ZSM-5. Note that CH_4 and NO + O_2 addition along the proposed pathways are most likely to proceed via adsorbed species: for CH_4 = [*CH_4], [z-*C]$_1$ and [z-*C]$_2$ (Scheme 2) and for NO + O_2 = mononitrosyl and activated oxygen over Co nanoclusters, respectively

located at the interface between oligonuclear cobalt oxidic species (or nanoclusters) and hydroxyl groups of the zeolite lattice, while nitrite species are preferably formed on large Co_xO_y particles (CoO and/or Co_3O_4), located on the surface or outside the zeolite crystals [18]. Based on all these statements, the reaction proceeds according to the two mechanistic pathways 1 and 2 presented in Scheme 3.

The activity of mononitrosyl NO on Co sites with respect to methane is negligible as follows from the equality of summarized rates of $NO_2^{\delta+}$ and nitrite conversion and the total rate of NO reduction into N_2. This has also been concluded by other authors [4,20] where NO_x ($x = 2$ or 3) surface species are considered as the only reaction intermediates. However, the fact that mononitrosyls are not able to activate methane does not enable one to exclude the possibility that part of these species can participate in the reaction due to their conversion into nitrite complexes, likely after migration from isolated sites to the cobalt oxide particles (see Scheme 1).

It can be discussed at this stage how the mechanism proposed from this SSITKA investigation (Scheme 3) compares with the mechanisms most often discussed in the literature for deNO_x reaction. Most of deNO_x SCR mechanisms can be classified into two groups: “decomposition” and “reduction” mechanisms. In the first case N_2 formation results from NO decomposition on reduced sites containing oxygen vacancies, which, in turn, after being oxidized by the NO decomposition, are rereduced by the hydrocarbon [21–23]. This “decomposition” scheme is totally unlikely in our case since DRIFT and TAP transient kinetic experiments [15] have excluded the possibility of NO_x decomposition to form N_2 in the absence of methane. It can therefore be concluded that namely $NO_2^{\delta+}$ and NO_2^- species directly react with CH_4. This scheme corresponds to the reduction mechanism, which includes N_2 formation originated from a series of consecutive transformations with participation of two reacting agents. There are four variants of such elementary steps: (i) NO reaction with adsorbed carbon species formed from hydrocarbon [24]; (ii) NO reaction with partially oxidized hydrocarbon [21,23,25]; (iii) hydrocarbon reaction with NO_x complexes formed due to NO oxidation [2,3,6,8,21,23]; (iv) reaction of NO_x complexes with carbonaceous species (“bifunctional mechanism”) [26]. Mechanisms (i)

and (ii) can most likely be discarded, because NO instead of CH_4 forms strong adsorbed complexes in our case. Our reaction scheme is thought to be closer to mechanism (iii) (with gaseous CH_4), or even better from mechanism (iv) since it involves the participation of both weakly bound methane (noted [*CH_4] in Scheme 2, as reversibly adsorbed methane), and activated complexes resulted from CH_4 irreversible conversion into CO_2 (noted [z-*C]$_1$ and [z-*C]$_2$ in Scheme 2).

According to our modeling results, the reaction pathway via $NO_2^{\delta+}$ adspecies (pathway 1 in Scheme 3) is ~ 2.5 faster than that occurring via nitrite complexes (pathway 2 in Scheme 3). Since the number of the active sites in pathway 1 (oxidic Co nanoclusters in tight interaction with OH species) is only 10% of the total amount of cobalt in the catalyst, it can be inferred that the intrinsic rate per active site is about 25 times higher in pathway 1 than in pathway 2. However, if one compares the ratio between the rate of $NO_2^{\delta+}$ interaction with methane and their concentration with the same ratio for nitrite complexes, it seems that the rate constant of nitrite interaction expressed by this mode is at least not lower than that for $NO_2^{\delta+}$ species. In other words, nitrite complexes are not less reactive with respect to methane than $NO_2^{\delta+}$. Comparatively the low overall rate of the reaction proceeding via nitrite complexes (pathway 2), considering their relatively high activity with respect to methane, can be caused by two factors: (i) a low rate of formation and/or (ii) a low conversion rate of C,N-containing intermediates resulted from nitrite reaction with methane. It is obvious that the first factor predominates in our experiments: the concentration of nitrite complexes drops to zero under SCR conditions, indicating that their reaction with methane proceeds very fast. Accordingly, the rate-limiting step of pathway 2 is the nitrite formation.

As for pathway 1 proceeding via $NO_2^{\delta+}$ intermediates, Table 2 has shown that the concentration of $NO_2^{\delta+}$ species decreases appreciably in comparison with that under adsorption–desorption equilibrium, but does not fall to zero. This concentration is raised with oxygen content in the reaction mixture, i.e., these species are not able to completely react with methane. It is not straightforward to unambiguously identify the rate-limiting step in this case, which can be tentatively assigned to the interaction of $NO_2^{\delta+}$ with methane. According to the literature [2–14], the interaction of adsorbed NO_x complexes with CH_4 is generally assumed to be the rate-limiting step in this reaction. According to our results, this holds only for one route (pathway 1); nevertheless, since this route is dominant, total reaction rate should be limited by the rate of methane activation. In this respect our data do not contradict the other results in the literature.

4.3. Intrinsic activity of active sites and reacting intermediates

Concerning to the nature of the most active sites in the SCR of NO with CH_4 over Co-ZSM-5, our results indicate that not only do cobalt sites play a major role per se, but they also act in combination with acid sites. The nuclearity and specific location of the cobalt entities in close vicinity of the acidic sites remains a very challenging aspect in this deNO_x catalysis. An advanced molecular description of these most active sites located at channel intersection is proposed in [18]. Indeed, turnover number of the reaction on the nanocluster sites interacting with zeolite OH groups is about 25 times higher than that on larger cobalt oxide particles located outside the zeolite channels. Kinetically, an influence of the acid sites is not revealed on the step of interaction with methane (as was shown above, the rates of this step for $NO_2^{\delta+}$ and nitrites are comparable), but it becomes apparent mainly on the step of NO_x complex formation. In this case the intrinsic formation rate (or turnover frequency referred to one active site) of $NO_2^{\delta+}$ species stabilized in the zeolite channel with participation of OH groups is several orders of magnitude higher than that of nitrite complexes [1]. A confinement effect which would gather on the same nanocluster $NO_2^{\delta+}$ species stabilized by OH groups, and methane adspecies to form the intermediate complexes CNO_xH_y able to react in turn with another NO adspecies to form gaseous N_2 and CO_2 is likely to explain this unique intrinsic rate.

The proper nature of the activated methane intermediates noted [z-*C]$_1$ and [z-*C]$_2$ in Scheme 2 (or CH_4 in Scheme 3) and which concentrations are reported in Table 3 remains unclear. From IR studies reported in [18], the formation of methoxy radicals (CH_3–O) both on CoO nanoclusters and cobalt oxide particles is most likely under SCR conditions. These methoxy species would react with the close NO_x adspecies ($NO_2^{\delta+}$ or nitrite) following the above-described SCR pathways. Eventually, they could also be oxidized directly into CO_2, especially at higher temperatures when the concentration of NO_x adspecies is decreasing. This would explain the decrease in N_2 yield at high temperature as observed in Fig. 1 [18].

Numerical analysis of the dynamics of ^{18}O label transfer provides valuable information to further unravel the reaction mechanism. It was shown in our previous works that $NO_2^{\delta+}$ formation is preceded by reversible and dissociative oxygen adsorption, the rate of this step being very low (about 10^{16} molec/(g s)) [1,27]. In principle, the rate of oxygen adsorption should limit the rate of $NO_2^{\delta+}$ formation under the reaction conditions. However, according to our estimations, the rate of the reaction proceeding with participation of $NO_2^{\delta+}$ species exceeds the value of 10^{17} molec/(g s). Thus, it seems that the formation rate of the oxidized sites participating in $NO_2^{\delta+}$ production increases under the reaction conditions. On the other hand, the experiments with labeled oxygen show that the rate of ^{18}O-label transfer into the catalyst is also raised. According to numerical analysis results, this increase is not only due to the isotope exchange with the reaction products, but also caused by the appearance of an additional pathway of the label transfer concerned with the steps of the catalytic cycle. It can be proposed that this acceleration of ^{18}O-label transfer into the catalyst active

phases is directly associated with the increase of the formation rate of the oxidized sites. But this situation can only occur if oxygen from the oxidized sites participates in the catalytic cycle and is transferred into the reaction products; then, the label transport into the catalyst accompanies the reoxidation step. Reoxidation of the active sites by molecular oxygen is likely to proceed simultaneously with formation of the products, and the active sites can be reoxidized (i.e., regenerated) by both O_2 and NO. This scheme of the reaction mechanism allowed us to simulate all the data obtained in SSITKA experiments with both labeled NO and labeled O_2.

5. Conclusions

A steady-state isotopic transient kinetic analysis (SSITKA) technique has been applied to investigate the reactivity of adsorbed NO_x complexes on different cobalt species in Co-ZSM-5 with methane in the presence of oxygen. Numerical analysis of the responses during isotopic switches of $^{14}N^{16}O \rightarrow {}^{15}N^{18}O$, $^{16}O_2 \rightarrow {}^{18}O_2$, and $^{12}CH_4 \rightarrow {}^{13}CH_4$ was performed. The concentrations of various adsorbed NO_x species on the catalyst surface, including mononitrosyls, nitrites, and $NO_2{}^{\delta+}$ species and their relative reaction rates with methane were determined. In addition, the concentrations of surface intermediates resulting from NO_x interaction with methane were also estimated. The SCR of NO with CH_4 into N_2 and CO_2 proceeds via two differentiated pathways: (1) with participation of $NO_2{}^{\delta+}$ species formed at the interface between oligonuclear cobalt oxidic species and hydroxyl groups of the zeolite lattice and (2) with participation of nitrite complexes on larger cobalt oxide particles located outside the zeolite channels. Mononitrosyl species adsorbed on isolated Co ions were found not to be directly active for activation of methane, although they can participate in the overall reaction by interconversion to nitrite species. $NO_2{}^{\delta+}$ species and nitrite complexes have similar reactivity with respect to methane. The higher reaction rate of pathway 1 is caused by a substantially higher rate of $NO_2{}^{\delta+}$ formation in comparison with that for nitrites in pathway 2 under the reaction conditions studied.

Acknowledgments

This work was carried out within the Twinning Program between the Institut de Recherches sur la Catalyse (Villeurbanne, France) and the Boreskov Institute of Catalysis (Novosibirsk, Russia). This work was partially supported by Russian Fund of Basic Research, Grant 00-03-22004.

Appendix A. Notation

C_i	Concentration of gas-phase i species, vol%
$E(CH_4)$	CH_4 efficiency in SCR process
F	Volumetric flow rate, ml/s
N	Avogadro number (6.023×10^{23}), molec/mol
t	Time, s
V	Reactor volume, cm^3
$\overrightarrow{w}_{jk}$	Rate of formation of adsorbate j in reaction k, molec/(g_{cat} s)
$\overleftarrow{w}_{jl}$	Rate of decomposition of adsorbate j in reaction l, molec/(g_{cat} s)
W	Catalyst weight, g
α_i	Isotopic fraction of gas-phase i species
α_j	Isotopic fraction of adsorbed j species
ξ	Dimensionless bed length
θ_j	Concentration of adsorbate j, molec/g_{cat}

References

[1] E.M. Sadovskaya, A.P. Suknev, L.G. Pinaeva, V.B. Goncharov, B.S. Bal'zhinimaev, C. Chupin, C. Mirodatos, J. Catal. 201 (2001) 159.
[2] Y. Li, T.L. Slager, J.N. Armor, J. Catal. 150 (1994) 388.
[3] A.T. Bell, Catal. Today 38 (1997) 151.
[4] A.W. Aylor, L.J. Lobree, J.A. Reimer, A.T. Bell, Stud. Surf. Sci. Catal. 101 (1996) 661.
[5] B.J. Adelman, T. Beutel, G.-D. Lei, W.M.H. Sachtler, J. Catal. 158 (1996) 327.
[6] A.D. Cowan, R. Dumpelmann, N.W. Cant, J. Catal. 151 (1995) 356.
[7] F. Witzel, G.A. Sill, W.K. Hall, J. Catal. 149 (1994) 229.
[8] V.A. Sadykov, S.A. Beloshapkin, E.A. Paukshtis, G.M. Alikina, D.I. Kochubei, S.P. Degtyarev, N.N. Bulgakov, S.A. Veniaminov, E.V. Netyaga, E.V. Bunina, A.N. Kharlanov, E.V. Lunina, V.V. Lunin, V.A. Matyshak, A.Ya. Rozovskii, Polish J. Environ. Stud. 6 (1997) 21.
[9] A.D. Cowan, N.W. Cant, B.S. Haynes, P.F. Nelson, J. Catal. 176 (1998) 329.
[10] E.A. Lombardo, G.A. Sill, J.L. d'Itri, W.K. Hall, J. Catal. 173 (1998) 440.
[11] D.B. Lukyanov, J.L. d'Itri, G. Sill, W.K. Hall, Stud. Surf. Sci. Catal. 101 (1996) 651.
[12] A. Boix, R. Mariscal, J.L.G. Fierro, Catal. Lett. 68 (2000) 169.
[13] X. Wang, H.Y. Chen, W.M.H. Sachtler, Appl. Catal. B 29 (2001) 47.
[14] X. Wang, H.Y. Chen, W.M.H. Sachtler, J. Catal. 197 (2001) 281.
[15] L.G. Pinaeva, E.M. Sadovskaya, A.P. Suknev, V.B. Goncharov, V.A. Sadykov, B.S. Balzhinimaev, T. Decamp, C. Mirodatos, Chem. Eng. Sci. 54 (1999) 4327.
[16] J. Happel, Isotopic Assessment of Heterogeneous Catalysis, Academic Press, 1986.
[17] C. Mirodatos, Catal. Today 9 (1991) 83.
[18] C. Chupin, PhD dissertation, Lyon 1 University (2001).
[19] E.M. Sadovskaya, D.A. Bulushev, B.S. Bal'zhinimaev, Kinet. Katal. 40 (1999) 61.
[20] C. Shi, M.J. Cheng, Z.P. Qu, X.F. Yang, X.H. Bao, Appl. Catal. B 36 (2002) 173.
[21] M. Iwamoto, H. Yahiro, Catal. Today 22 (1994) 5.
[22] R. Burch, P.J. Millington, Catal. Today 29 (1996) 37.
[23] H. Hamada, Catal. Today 22 (1994) 21.
[24] K.C.C. Kharas, Appl. Catal. B 2 (1993) 207.
[25] J. Vassallo, E. Miro, J. Petunchi, Appl. Catal. B 7 (1995) 65.
[26] P. Ansell, A.F. Diwell, S.E. Golunski, J.W. Hayes, R.R. Rajaram, T.J. Truex, A.P. Walker, Appl. Catal. B 2 (1993) 81.
[27] B. Wichterlovà, J. Dědeček, Z. Sobalík, in: G. Centi, et al. (Eds.), Catalysis by Unique Metal Ion Structures in Solid Matrices, Kluwer Academic, Dordrecht, 2001, pp. 31–53.